Effect of Film Thickness and Domain Spacing on Defect Densities in Directed Self-Assembly of Cylindrical Morphology Block Copolymers

Vindhya Mishra,[†,§] Glenn H. Fredrickson,[†,‡] and Edward J. Kramer[†,‡,*]

[†]Department of Chemical Engineering and [‡]Department of Materials, University of California, Santa Barbara, California 93106, United States. [§]Present address: DuPont Central Research and Development, Wilmington, Delaware 19880.

ABSTRACT Directed assembly of block copolymer thin films is recognized as a high-throughput, low-cost complement to optical lithography with the ability to overcome the 32 nm natural resolution limit of conventional lithographic techniques. For bulk block copolymer systems, desired feature sizes ranging from 5 to 100 nm can be obtained by controlling the molecular weight and composition of a block copolymer, as long as the bulk order—disorder temperature (ODT) is such that the copolymer is well-segregated at the processing conditions. However, our studies on graphoepitaxially aligned cylindrical morphology block copolymer monolayer and bilayer films demonstrate that, as domain sizes are reduced, the block copolymer becomes increasingly susceptible to an unacceptably high density of thermally generated defects, resulting in a significant reduction of the ODT. Thus, in thin films, the minimum feature spacing accessible is limited by thermal defect generation and not by the bulk ODT. Our experimental studies on monolayer films of cylindrical morphology polystyrene-*b*-poly(2-vinyl pyridine) with microdomain spacings approaching 20 nm reveal that defect densities and the ODT are surprisingly sensitive to variations as small as 2 nm in the microdomain spacing. Additionally, the monolayer and bilayer ODT differ by nearly 100 °C when the monolayer domain spacing is 20 nm, while the difference is only 20 °C when the monolayer domain spacing is 22 nm. We explain this behavior using a quantitative estimation of the energetic cost of defect production in terms of the domain spacing, χN, and block copolymer composition. These studies reveal unexpected consequences on the equilibrium defect densities of thin film block copolymers which must be accounted for when designing a block-copolymer-based directed-assembly process.

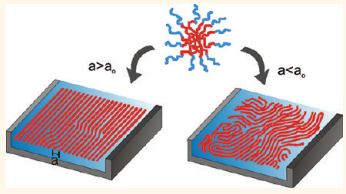

KEYWORDS: block copolymer · lithography · defects · thin films · directed self-assembly · graphoepitaxy

Integration density of silicon chips has witnessed a steady growth over the past few decades with simultaneous reduction in the cost per chip. While the means for patterning has essentially remained optical lithography, device miniaturization by resolution enhancement techniques and use of smaller wavelength sources has brought down the critical length scale of devices from the micrometer scale to 160 nm on a routine basis today.[1] However, this rate of growth cannot been maintained indefinitely as the industry is approaching the fundamental resolution limit for optical lithography, and attaining a pitch size smaller than 32 nm is proving to be increasingly expensive. The international roadmap for semiconductors has identified devising an efficient and relatively cheap route to overcome this resolution limit as one of the biggest challenges faced by the semiconductor industry.[2] Block copolymers are being considered as a potential solution to this problem, particularly for dynamic random access memories and potentially for circuit fabrication, as well. The spontaneously formed dense array of nanometer-sized domains in block copolymer systems can be used as templates for subsequent patterning operations. Successful examples of block-copolymer-assisted fabrication include creation of quantum dots,[3] magnetic storage media,[4] semiconductor capacitors,[5] or nanowires.[6–8] Moreover, the processing steps involved in block-copolymer-assisted fabrication, namely, spin coating, thermal annealing treatment, and dry etching, are already a part of existing manufacturing lines for photoresist treatment, which can facilitate easy integration of block copolymer lithography into existing facilities.

However, in the absence of an external guiding force, the patterns formed by block copolymer assembly typically consist of randomly oriented grains with a considerable density of defects. Thermally excited long wavelength phonon modes are sufficient to destroy long-range order in infinite 2D hexagonal lattices (spherical morphology block copolymers and vertically oriented cylinders)

* Address correspondence to edkramer@mrl.ucsb.edu.

Received for review December 30, 2011 and accepted February 7, 2012.

Published online February 17, 2012
10.1021/nn205120j

and 2D and 3D smectics (lamella and monolayers of horizontally oriented cylinders).[9−11] There have been several efforts to direct alignment in the microdomains through use of an external field such as chemical[12] and topographical patterning,[13] electric field,[14] flow,[15] or application of shear.[16] Of particular interest is graphoepitaxy, first demonstrated by Segalman and co-workers[13] for spherical morphology block copolymers and by Sundrani and co-workers for cylinder-forming systems,[17] where coarse scale patterns created using conventional photolithography can direct alignment of the block copolymer domains on a finer scale, driven either by the tendency of one of the close packed rows of the pattern to align parallel to an edge[4,13] or by the preferential wetting of the pattern walls by one of the blocks.[17,18] The physical confinement on a lateral scale may also cut off the long wavelength phonon modes that are responsible for destruction of order.

Even though these epitaxial techniques can direct long-range *alignment* in the block copolymer microdomains, the resulting pattern is not free of *point defects* because of their low cost of generation. Previous studies indicate that defects are in the form of dislocations at low temperatures and disclinations as the order−disorder temperature is approached.[19−22] In infinite 2D lattices exhibiting six-fold symmetry (spheres and cylinders aligned perpendicular to the substrate), dislocations always occur as bound pairs because their energy as isolated defects diverges with the size of the system, while in smectic-like patterns (parallel cylinders or lamella), isolated dislocations have finite energy.[20,21] However, microelectronics fabrication requires high fidelity in pattern shape, domain size, and placement; for example, defect tolerance in bit-patterned media is of the order of 1 in 10^{4-6} dots.[18] Achieving defect-free block copolymer patterns over large areas using epitaxy demands relatively tight restrictions on the coarse directing pattern,[12,20,23,24] which cannot be easily realized using common fabrication techniques. While several efforts have focused on improving guiding techniques to direct alignment and achieve long-range order in block copolymer patterns,[25−27] it is also important to investigate the influence that the intrinsic properties of the block copolymer may have on defect densities, as that may supersede any external influences. This will also assist in selecting an appropriate block copolymer for patterning applications. The annealing temperature of block copolymers is another important processing parameter that significantly affects the quality of the pattern and the processing time. While kinetics of defect removal during annealing are expedited by higher processing temperatures, as we approach the bulk order−disorder transition (ODT) temperature, the density of thermally generated defects will also increase. One can imagine that the bulk ODT temperature must provide an upper limit T_m for processing

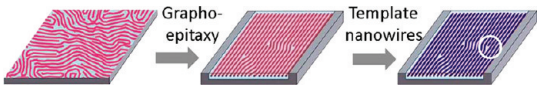

Figure 1. Fabrication of dense arrays of nanowires using directed self-assembly.

temperature—a temperature at which the density of defects is increased to the extent that the arrangement of the microdomains is completely disordered. However, for nanolithography applications, the block copolymer is typically in the form of a resist-like thin film, and as thin film equilibrium behavior has been seen to be different from that of the bulk,[20,28,29] the bulk ODT may not be an accurate estimate for T_m.

To answer this set of questions, we have examined factors that affect T_m in thin films of graphoepitaxially aligned diblock copolymer cylinders layered parallel to the substrate. A recent study has demonstrated fabrication of dense arrays of metallic nanowires using a similar system,[6] as shown schematically in Figure 1. While for linear striped patterns, perpendicular lamellae-forming block copolymers are preferred over cylindrical morphology block copolymers for many industrial applications because of their better etch resistance, the parallel orientation of lamella with respect to the substrate is more commonly observed in experimental systems. Monolayers of cylindrical morphology block copolymers can produce similar features as perpendicular lamellar microdomains, with the advantage that the parallel orientation of cylinders is more common than cylinders oriented perpendicular to the substrate, and it exhibits faster kinetics of defect annihilation compared to lamella-forming block copolymers of similar molecular weight.[18] In our studies, we have probed the effect of microdomain spacing on defect densities in, and T_m of, monolayers and bilayers of cylinder-forming copolymers. In order to determine if the microdomain spacing affects equilibrium defect densities in block copolymer patterns, we compared the equilibrium structure in thin films of block copolymers with different natural domain spacings. As one of the aims of block copolymer assembly is to overcome the 32 nm limit of optical lithography, in our study, we used polymers designed such that the natural domain spacing of the block copolymer was smaller than that limit. Since we have defined T_m to be the temperature at which the epitaxially ordered array of microdomains converts into a disordered arrangement, for convenience, we shall refer to T_m as the thin film order−disorder transition temperature ($T_{ODT,f}$). The deviation of the thin film ODT from the bulk ODT was studied as a function of film thickness and microdomain spacing. Cylinder-forming block copolymers in a monolayer form a model 2D system compared to bulk block copolymer melts which form a 3D system. Moreover, the number of layers required to achieve true 3D behavior is not known. Hence a comparison

between T_{ODT} of a monolayer of cylinder-forming block copolymers with the bulk (3D) and bilayers (which cannot be characterized as either 2D or 3D systems) can help elucidate the effect of dimensionality on order−disorder transitions.

RESULTS

The block copolymer employed in this study is poly(styrene-*b*-2-vinyl pyridine) (PS-P2VP) with poly-(2-vinyl pyridine) as the minority block. Three block copolymers that differed in either their molecular weights or their composition were prepared by anionic polymerization. The cylinder spacing and order−disorder transition temperature in the bulk for these block copolymers were determined by temperature-dependent small-angle X-ray scattering (SAXS). For thin film studies, polymer films with thicknesses designed to produce either a monolayer or a bilayer of cylinders were spin coated on photolithographically patterned silicon wafers. The wafers were patterned with a 2 cm × 2 cm array of 2 μm wide silicon oxide channels separated by 2 μm wide mesas. These films were then subjected to thermal annealing under high vacuum conditions by heating above the bulk ODT to erase all processing history, then slowly cooled to the annealing temperature at a rate less than 0.05 °C/min and held for more than 1.5 days. The films were then cooled at a rate faster than 0.5 °C/min to room temperature before removing from vacuum. The structure of the films was imaged using atomic force microscopy, and grazing incidence small-angle X-ray scattering (GISAXS) was used to obtain statistically representative structural data averaged over large areas.[28,30−32]

The three PS-PVP block copolymers used in this study are PS-PVP$_{0.22}$ (M_n ∼ 21 kg/mol, minority block volume fraction ϕ_{PVP} = 0.217, polydispersity index (PDI) = 1.085), PS-PVP$_{0.23}$ (M_n ∼ 21 kg/mol, ϕ_{PVP} = 0.232, PDI = 1.09), and PS-PVP$_{0.26}$ (M_n ∼ 26 kg/mol, ϕ_{PVP} = 0.258, PDI = 1.075). The characterization data of the block copolymers are provided in the Supporting Information. The natural domain spacing in bulk was characterized using SAXS. SAXS profiles for samples annealed at 160 °C are shown in Figure 2. The average cylinder spacing in bulk, which is related to the first-order peak position q^* in SAXS by $a = 4\pi/\sqrt{3}q^*$, was calculated to be 22.1 ± 0.5, 23.7 ± 0.5, and 24.6 ± 0.5 nm, respectively. Hence the block copolymers differ only slightly in terms of their nearest neighbor spacing. The bulk order−disorder transition temperatures were determined using temperature varying SAXS measurements, where the ODT is characterized by a sharp drop in the intensity and significant broadening of the first-order Bragg peak. As an example, temperature varying SAXS data for the PS-PVP$_{0.22}$ copolymer are shown in Figure 3, while the data for the other two block copolymers can be found in the Supporting Information. The ODTs for PS-PVP$_{0.22}$, PS-PVP$_{0.23}$, and PS-PVP$_{0.26}$ were determined to be 195 ± 10, 210 ± 5, and 260 ± 10 °C, respectively. This trend is consistent with the block copolymer molecular weights and volume fractions, given the universality in bulk block copolymer behavior in terms of χN and the volume fraction of the minority block.

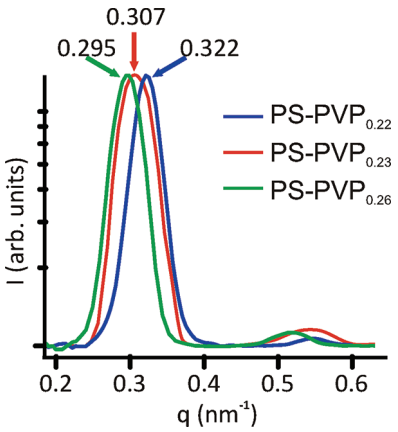

Figure 2. Line profiles obtained by azimuthal integration of the 2D X-ray scattering maps for bulk samples of the PS-PVP$_{0.22}$, PS-PVP$_{0.23}$, and PS-PVP$_{0.26}$ copolymers at 160 °C. The microdomain spacing in bulk is related to the inverse of the first-order peak position.

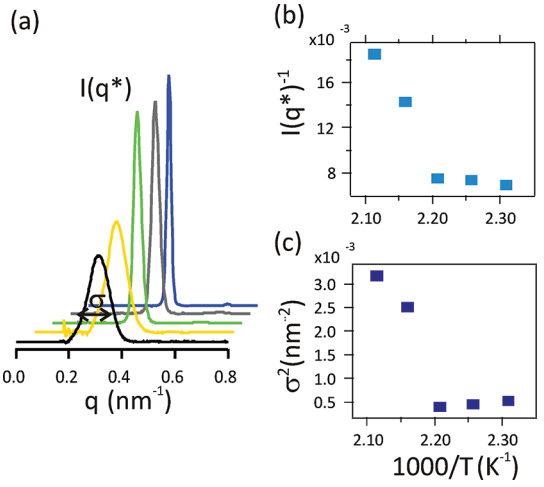

Figure 3. (a) Variation of intensity with scattering wave vector for a bulk sample of the PS-PVP$_{0.22}$ polymer obtained by azimuthal integration of the scattering patterns at various temperatures. The sharp drop in intensity (b) and broadening of the first-order peak (c) demarcates the order−disorder transition temperature.

In the next section, we address the order−disorder transition in thin films, specifically films consisting of either a monolayer or a bilayer of microdomains. We used scanning probe microscopy to image the structure of the films that had been subjected to rigorous thermal annealing treatments at different temperatures. Figure 4 shows the sequence of steps leading to disorder in a monolayer of the PS-PVP$_{0.23}$ polymer annealed at different temperatures. The behavior we observe here is

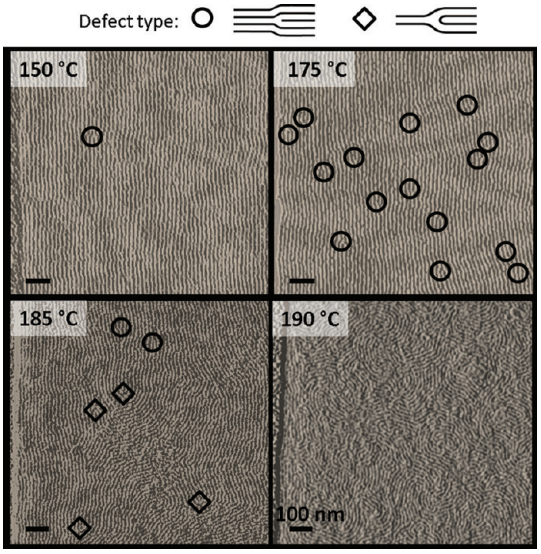

Figure 4. Nature of the order–disorder process in 2D for cylindrical morphology block copolymer. Shown here are atomic force micrographs for a monolayer of the PS-PVP$_{0.23}$ block copolymer. The transition process is mediated by thermal generation of dislocations, which unbind into disclinations at higher temperatures. The circles are examples of dislocations, while the diamonds show a few disclination pairs.

consistent with previous studies by Hammond *et al.*,[20] where at temperatures much lower than the bulk ODT of 210 °C, the cylindrical microdomains show nearly perfect alignment with the channel walls; however, a finite density of defects can be detected in the system even at annealing temperatures 60 °C lower than the bulk ODT. The defects are exclusively dislocations, whose density increases as the annealing temperature is increased. As the bulk ODT is approached, unbinding of the dislocation into pairs of disclinations takes place, resulting in complete disorder when the disclination density becomes greater than about 20/μm^2. The system first loses its translational order by generation of dislocations and then its orientational order by generation of disclinations. This behavior is analogous to the smectic to nematic to isotropic transition exhibited by liquid crystals, where the microdomains in monolayers of cylindrical morphology block copolymers are analogous to the smectic layers. Atomic force micrographs of bilayer thick films (see Supporting Information) also showed a similar sequence where the order–disorder transition was mediated by generation of dislocations and disclinations; however, the temperature at which the film disordered was higher than that for the monolayer. We shall refer to the temperature at which both translational and orientational order is lost in a thin film as the "ODT", although evidently microphase separation of the blocks is still present when slightly above that threshold. This distinction between the ODT and the loss or onset of microphase separation is not as apparent in bulk block copolymer systems.

In order to study the effect of microdomain spacing and film thickness, we compared the ODT temperature for monolayers and bilayers of the three block

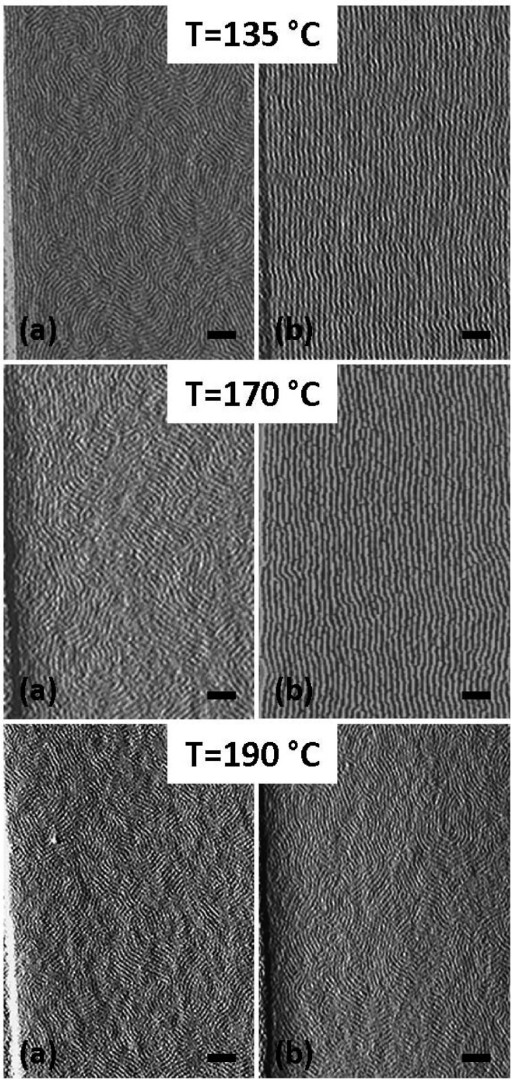

Figure 5. AFM micrographs for monolayer thick films of (a) PS-PVP$_{0.22}$ and (b) PS-PVP$_{0.23}$ copolymers as a function of temperature. The monolayer ODT for the PS-PVP$_{0.23}$ block copolymer is 35 °C lower than its bulk ODT, while that for the PS-PVP$_{0.22}$ block copolymer is more than 90 °C lower than the PS-PVP$_{0.22}$ bulk ODT. Scale bar = 100 nm.

copolymers and found unexpected differences. Using GISAXS and atomic force microscopy, the in-plane microdomain spacings for monolayers of PS-PVP$_{0.22}$, PS-PVP$_{0.23}$, and PS-PVP$_{0.26}$ copolymers were determined to be 20.3 ± 0.5, 22.3 ± 0.5, and 24.2 ± 0.5 nm, respectively. Atomic force micrographs for the PS-PVP$_{0.22}$ and PS-PVP$_{0.23}$ block copolymers annealed at different temperatures are shown in Figure 5. The PS-PVP$_{0.23}$ monolayer ODT occurred at 190 ± 5 °C, which is 20 °C less than the bulk ODT temperature. However, the PS-PVP$_{0.22}$ monolayer showed completely isotropic arrangement of its microdomains even at temperatures as low as 120 °C, which is about 75 °C lower than its bulk ODT temperature. As the glass transition temperatures of polystyrene and poly(2-vinyl pyridine) are both about 100 °C, annealing temperatures lower than that limit could not be employed.

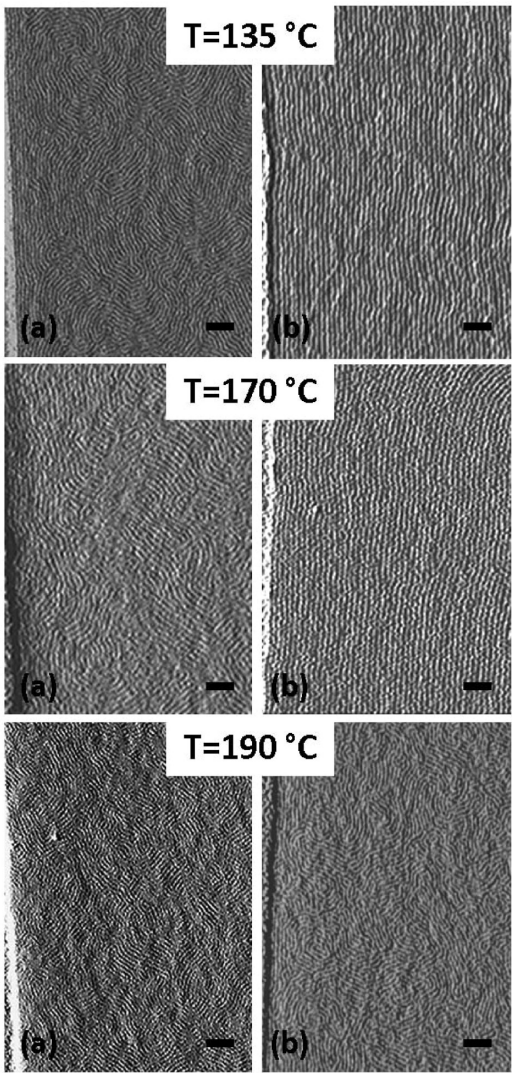

Figure 6. Contrast between the melting behavior of the (a) monolayer *vs* (b) bilayer for the PS-PVP$_{0.22}$ block copolymer. The monolayer ODT is more than 75 °C lower than its bulk ODT, while the bilayer ODT is only 5 °C lower than the PS-PVP$_{0.22}$ bulk ODT. Scale bar = 100 nm.

Hence, while the bulk ODT temperatures for the two block copolymers differ by 10 °C, their monolayer order−disorder transition temperatures differ by more than 70 °C. In all previous works on graphoepitaxy, there has been no report where the orientation of the copolymer microdomains were unaffected by epitaxy as long as the annealing temperature is below the bulk order−disorder transition temperature and above the glass transition temperature. In fact, Hammond *et al.*[33] reported that even above the order−disorder transition temperature the microdomains in the cylinder-forming block copolymer closest to the hard edge still retain their orientation along the edge. Hence, the behavior of PS-PVP$_{0.22}$ monolayer is unexpected. The ODT for the PS-PVP$_{0.26}$ monolayer was determined to be 235 °C, 30 °C lower than its bulk ODT.

Even more remarkably, the bilayer of the same PS-PVP$_{0.22}$ block copolymer showed almost perfect

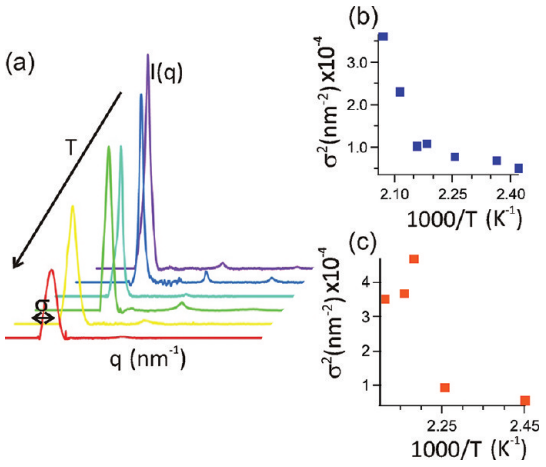

Figure 7. (a) In-plane scattering profiles for a bilayer of the PS-PVP$_{0.22}$ polymer obtained by grazing incidence scattering, at various temperatures. (b) Full width at half-maximum of the first-order peak for PS-PVP$_{0.22}$ bilayer as a function of temperature. (c) Full width at half-maximum of the first-order peak for a PS-PVP$_{0.23}$ monolayer as a function of temperature.

alignment at 130 °C with fewer defects than 1 defect per 20 μm^2 area, even though some defects originate from visible dirt or wall edge roughness (Figure 6). The bilayer loses its order by unbinding of disclinations at 190 ± 5 °C, which is very close to the bulk ODT temperature. Hence a monolayer and bilayer of the same block copolymer show drastically different defect densities at the same temperature. Bilayers of PS-PVP$_{0.23}$ and PS-PVP$_{0.26}$ polymers also disorder at a temperature higher than that of their corresponding monolayers; however, the extent of depression of the monolayer ODT seems to vary strongly depending on the block copolymer.

Ideally, a reliable quantification of the positional and orientational order in the block copolymer thin films can be obtained using X-ray scattering in the grazing incidence mode, where the elongated path of the beam through the film compensates for the low contrast and small polymer volume resulting in intense scattering even from very thin films when high-energy synchrotron sources are used. Each sample was first aligned with the channel walls parallel to the direction of the incident X-ray beam by rotating the sample in the azimuthal direction Φ about the sample normal (see Figure 14). Line profiles extracted from 2D scattering images for samples annealed at different temperatures for the PS-PVP$_{0.22}$ bilayer and PS-PVP$_{0.23}$ monolayer in this $\Phi = 0$ position are shown in Figure 7. Positional order quantification can be extracted from the line shape of the first-order peak, while the order parameter quantifying orientational order can be measured by recording the intensity of the first-order peak as the sample is rotated in its plane. The details of this study are the subject of another publication.[34] Since a disordered state is characterized by short-ranged

TABLE 1. Order–Disorder Transition Temperatures and Microdomain Spacings for the Three Block Copolymers

block copolymer	monolayer cylinder spacing (nm)	monolayer ODT (°C)	bilayer ODT (°C)	bulk ODT (°C)
PS-PVP$_{0.22}$	20.3 ± 0.5	<110	190 ± 5	195 ± 5
PS-PVP$_{0.23}$	22.3 ± 0.5	190 ± 5	210 ± 5	220 ± 5
PS-PVP$_{0.26}$	24.2 ± 0.5	235 ± 5		260 ± 10

orientational order, we estimated the thin film ODT to be the temperature at which the orientational order showed a sudden drop. The temperatures thus estimated are in good agreement with the ODT estimation based on the atomic force micrographs of thin films. By combining the information extracted from GISAXS and the AFM micrographs, we determined the cylinder spacing in a monolayer and the order–disorder transition temperatures of monolayer, bilayer, and bulk for the three block copolymers, and the results are summarized in Table 1. The differences in the $T_{ODT,monolayer}$ for polymers with small differences in molecular weight and composition are striking. Monolayers of block copolymers that differ by just 2 nm in their microdomain spacing can exhibit ODT temperatures differing by 90 °C in the monolayer, while in the bulk, the difference in ODTs may be less than 15 °C.

DISCUSSION

Our experimental results show that, irrespective of the block copolymer molecular weight or minor block volume fraction, the monolayer films disorder at a lower temperature than bilayers, which disorder at temperatures close to but slightly lower than the bulk order–disorder transition temperature. The extent of depression of the monolayer ODT from the bulk appears to be strongly correlated to the nearest neighbor spacing. Literature review reveals one study[18] where lamellar-forming block copolymers with an intrinsic period of 32 nm formed a disordered structure under conditions where a cylinder-forming block copolymer with periodicity of 37 nm displayed much higher degree of order. However, no explanation was provided for this behavior. Moreover, using an oriented cylinder underlayer for the lamellar block copolymer stretched the periodicity of the lamellae to 35 nm, which showed drastically improved order.

One significant structural difference between bulk and thin films is the distortion of the unit cells associated with the microdomains as we confine the polymer to a thin film.[35] As shown schematically in Figure 8, the equilibrium unit cell associated with the cylindrical microdomains in the bulk phase is hexagonal, which gets distorted to a pentagon in a bilayer and a square in a monolayer. These distortions are expected to result in free energy penalties because of increased packing frustration of the polymer chains in the square and

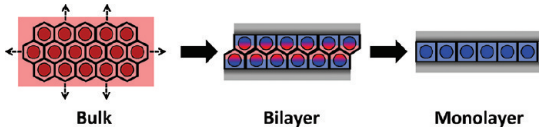

Figure 8. Confinement of cylindrical morphology block copolymer to thin films causes distortion of unit cell associated with each microdomain from hexagonal to square.

pentagon configuration compared to the six-fold symmetry of the hexagonal unit cell.

In order to confirm and quantify these differences, we used self-consistent field theory to calculate the free energy per chain for a AB cylinder-forming block copolymer in monolayer, bilayer, and bulk geometries as well as in the disordered (or completely mixed homogeneous) state as a function of χN, where χ is the temperature-dependent Flory–Huggins interaction parameter. While it is known that SCFT calculations break down close to the order–disorder transition due to neglect of thermal fluctuations, the motivation behind this treatment was to determine the relative free energies of the three geometries. The SCFT treatment followed here is detailed in an earlier paper.[36] We utilized a "masking" technique[37] to confine the polymer to a thin film bound by planar interfaces by imposing a "wall" density field that expels the polymer from the interface. In the simulations, for simplicity, we assumed symmetric boundary wetting conditions where the majority block was preferentially attracted toward both the polymer–substrate and polymer–air interfaces and the strength of the interaction parameter between the majority block and the interface was set equal to zero while the strength of the minority A block interaction with the wall χ_{AW} was set equal to χ_{AB}. The fraction of the minority block ϕ was fixed at 0.25. The free energy of the homogenously mixed state was approximated as the interaction energy $f_{dis} = \chi N\phi(1 - \phi)$.[38] As a rough approximation, the temperature at which the calculated free energy per chain in the ordered state became equal to that of homogenously mixed state was taken to be the order–disorder temperature.

The results of the SCFT calculations are shown in Figure 9. For a fixed block copolymer size N, at the same temperature, we find that $f_{monolayer} > f_{bilayer} > f_{bulk}$, where f is the free energy per chain, which is consistent with our expectations based on distortion of the unit cell. Hence, on the basis of our approximation, their ODT follows the opposite sequence $T_{ODT,monolayer} < T_{ODT,bilayer} < T_{ODT,bulk}$. Note that the definition of ODT assumed here deviates from our experimental definition of the thin film ODT where the two blocks are not completely mixed to lose all compositional order. From the SCFT calculations we obtain $\chi N_{ODT,monolayer} = 23.8$, $\chi N_{ODT,bilayer} = 20.5$, and $\chi N_{ODT,bulk} = 18$. Hence $\chi N_{ODT,monolayer} - \chi N_{ODT,bulk} = 6$, while $\chi N_{ODT,bilayer} - \chi N_{ODT,bulk} = 2.5$. Since χ is of the form (A/T)-B, for a block

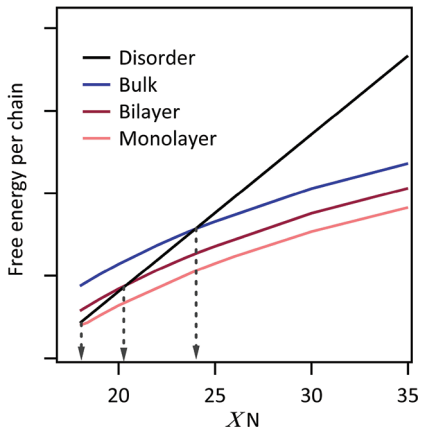

Figure 9. Differences in free energy per chain of the block copolymer in a monolayer, bilayer, and bulk phase, compared to the disordered state free energy.

copolymer with a degree of polymerization N, the order−disorder temperature for the monolayer can be estimated as

$$T_{ODT,monolayer} = \frac{AN}{23.8 + BN} \quad (1)$$

A similar estimate can be made for the bulk phase. Thus, the difference between the monolayer and bulk ODT will be of the form

$$T_{ODT,bulk} - T_{ODT,monolayer} = \frac{6AN}{(18 + BN)(23.8 + BN)} \quad (2)$$

According to this equation, the difference in the order−disorder transition temperatures of the monolayer and bulk increases weakly with increase in N. However, the SCFT simulations simply reveal the energetic penalty of distortion of unit cells and do not account for defects. Evaluating eq 2 for $N = 200$ using the Flory−Huggins interaction parameters $A = 63$ and $B = 0.033$ reported for the PS-PVP system, we find that $T_{ODT,monolayer}$ should be lower than that of the bulk by 100 °C. While this is much higher than our experimental value, the discrepancy could be due to the fact that the fluctuations that are not accounted for in mean-field theory will shift the ODT lower than the mean-field estimate. Moreover, our simulations treat the disordered state to be a homogenously mixed state, whereas in experiments, the disordered state still has compositional inhomogeneities (*i.e.*, microphase separation) with liquid-like arrangement of the cylindrical micelles. Furthermore, contrary to the assumption here, the free energy of the "disordered" state in thin films will be different from the "disordered" state in bulk, due to the presence of the surface.

Another possible explanation for the lower ODT exhibited by monolayers can stem from the pinning effects of adjacent layers on the orientational degrees of freedom of a given layer. Our definition of the ODT in thin films refers to loss of positional and orientational order rather than attaining compositional homogeneity. The cylindrical microdomains in a monolayer can wander in-plane more freely than in a bilayer where the corrugation imposed by the other layer would tend to produce energy barriers to bending/wandering of cylinders. This effect cannot be captured in our 2D SCFT simulation; however, it can explain the decrease in the ODT as the number of cylinder layers are reduced.

While the SCFT simulations do confirm that the distortion of the unit cells increases the free energy of the thin films relative to bulk, the treatment does not account for the energetics or entropy of defects. Since from Figure 4 it is evident that the disordering propagates by generation of point defects, in order to get a more accurate measure of $T_{ODT,film}$, we have to incorporate loss of order induced by defects in our calculation. Defects are generated when the energetic cost of producing the strain field of the defect is less than the free energy decrease due to the entropy gained by introduction of the defect. Since monolayers of block copolymer cylinders are similar to thermotropic smectic-A liquid crystals, we employed the elastic continuum theory that has been used in the past for layered smectic systems[20,39−42] to estimate the factors that affect the energetic cost of producing a defect. As dislocations are thermally generated point defects, their densities are expected to scale exponentially with their formation energy E_d

$$n_d \sim \frac{1}{a_c^2} \exp^{-E_d/k_B T} \quad (3)$$

where E_d is the energy of a single dislocation and a_c is the dislocation core radius. Note that isolated dislocations have finite energy in layered systems[43] unlike in hexagonal 2D crystals where the energy of isolated dislocations scales logarithmically with the size of the system.[44] If we consider a system consisting of a single grain of perfectly oriented cylinder cores, the inclusion of a defect in this structure gives rise to a strain energy field in the vicinity of the defect due to the bend and splay of the displaced microdomains. This strain field surrounding an isolated edge dislocation was first calculated by deGennes[42] and studied in detail by Pershan.[41] Accounting for the symmetries of the smectic-A phase and discarding elements of the distortion field that involve uniform translation or rotation, the elastic free energy density relative to the undistorted state in the first-order linear theory can be expressed as

$$F = \frac{1}{2} B \left(\frac{\partial u}{\partial z} \right)^2 + \frac{1}{2} K (\nabla \cdot \mathbf{n})^2 \quad (4)$$

where $\mathbf{n}$ is the local director normal corresponding to the direction of preferred orientation of the microdomains, K is the elastic constant corresponding to splay, and B is the compression modulus normal to the layers.

One can define a length scale $\lambda = (K/B)^{1/2}$ in terms of the two distortion elastic constants, which is known as the penetration depth. Assuming the displacement "*u*" does not vary in the film thickness direction "*y*", the displacement field *u* was evaluated by Chandrasekhar and Ranganath[39] by minimizing the total energy of the system $E = \int F dr$. The energy per unit length of an isolated dislocation can then be obtained as $\varepsilon_d = \int\int F dx dz$, where *F* is calculated for the dislocation field *u* using eq 4, which gives us the form

$$\varepsilon_d \sim \varepsilon_o + \frac{\lambda b^2 B}{2a_c} \quad (5)$$

where *b* is the length of the Burgers vector associated with the defect. Thus, the energy per unit length of a dislocation is composed of the energy of the dislocation core ε_o and the elastic strain energy around the defect. The length of the Burgers vector *b* is simply the in-plane cylinder spacing *a*. The penetration depth λ was estimated by Amundson and Helfland to be $\approx 0.25R_g$ for lamellar-forming block copolymer systems.[40] From our SCFT calculations, $a \sim 4R_g$, hence we can approximate λ as 0.06*a*. The total energy associated with a defect E_d is obtained by multiplying the energy per unit length ε_d by the depth of the defect. The interlayer spacing in cylinder-forming block copolymers is about *a* for a monolayer and 0.866*a* for bilayers, hence the depth of the defect scales as *na*, where *n* is the number of layers. Using $a_c \sim a$, we obtain the following form for the defect density E_d

$$E_d = na\varepsilon_o + 0.03na^3B \quad (6)$$

Thus, if we ignore the contribution of the core energy as is usual in dislocation theory, E_d scales approximately as a^3. Since the number density of defects decreases exponentially with E_d (eq 3), we can expect a small change in the characteristic spacing *a* to have dramatic effects on the defect densities, depending on the magnitude of the compression modulus *B*. From the GISAXS data, the characteristic cylinder spacing in the monolayer of each block copolymer at 140 °C was found to be 20.3, 22.3, and 24.2 nm for PS-PVP$_{0.22}$, PS-PVP$_{0.23}$, and PS-PVP$_{0.26}$, respectively. Assuming *B* to be a linear function of temperature $B = B^\circ - B'T$, by fitting defect densities obtained from atomic force micrographs *versus* temperature for the PS-PVP$_{0.23}$ monolayer, $0.03a^3B^\circ$ was estimated for the PS-PVP$_{0.23}$ block copolymer monolayer by Hammond *et al.* to be $6000k_B$;[20] that is, E_d is approximately $14k_BT$. Assuming *B* to be a function of temperature alone, the number density of dislocations for the three block copolymers can then be calculated using a simple scaling argument from eq 3, and these are shown in Figure 10. The large differences in the values for dislocation density arising from a 2 nm difference in microdomain spacing show that small variations in polymer size and composition can lead to drastic differences in the thin film T_{ODT}. The general form of E_d for PS-PVP cylinder-forming block copolymer monolayers can be approximated as $E_d \sim 0.0013k_BTa^3$, where *a* is in nanometers. Note that since E_d scales linearly with the depth of the defect (*i.e.*, the number of layers), the dislocation energy for a bilayer would be nearly twice that of the monolayer and hence the dislocation density at the same temperature would decrease dramatically as the film thickness is increased. Although formally bilayers are similar to columnar liquid crystals instead of smectics, the form of the strain energy has the same dependence on *a*.[45]

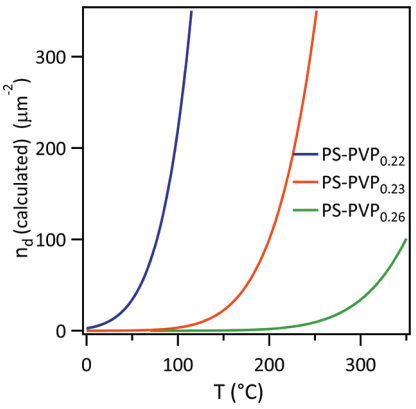

Figure 10. Dependence of defect density on microdomain spacing for monolayer films as estimated by eq 6.

Although the above calculation calculates density of dislocations only and does not take disclinations into account, it has been predicted theoretically[46] and observed experimentally[20] that the density of disclinations which arise from the unpairing of disclinations that comprise the dislocations only can increase once the dislocation density reaches a certain level $n_{d,*}$. An estimate for T_{ODT} that accounts for dislocation defects can be obtained by comparing the temperature at which the number density of dislocations becomes larger than $n_{d,*}$. On the basis of the data extracted from atomic force micrographs for the PS-PVP$_{0.23}$ monolayer, $n_{d,*} \approx 40\ \mu m^{-2}$. This estimated temperature scales as $a^3/k_BLn(a^2n_{d,*})$. This implies that as the microdomain spacing of the block copolymers becomes smaller, the monolayer ODT temperature decreases much faster than the form $AN/(23.8 + BN)$ predicted by eq 1 based on distortion of the unit cell upon confinement, which is consistent with our experimental observations.

Since the calculations above depend on the E_d extracted from quantitative analysis of atomic force micrographs, we wanted to obtain an independent estimate for E_d. As can be seen from eq 5, the energy of the defect also scales linearly with the layer compression modulus *B*. In order to determine the effect of various factors on *B*, we used self-consistent field theory to calculate *B*, similar to the approach adopted

by Hammond *et al.*[20] The compression modulus B can be estimated by calculating the change in energy per chain f when the layer dimensions are changed by small strain amounts ε.

$$\frac{\Delta f}{k_B T} = \frac{B\bar{V}}{2RT}\varepsilon^2 \quad (7)$$

where $\bar{V}$ is the molar volume of the copolymer. Unlike Hammond and co-workers who calculated the compression modulus using a square unit cell with periodic boundary conditions in all directions, we simulated the thin film geometry by confining in the film thickness direction by imposing a "wall" density profile. Since both a and B for a monolayer can be obtained from SCFT, we can obtain a theoretical estimate for E_d using $E_d \sim 0.03na^3B$. For simulation conditions designed to mimic the experimental conditions of PS-PVP$_{0.23}$ block copolymer, we obtain $E_d = 5428k_B$, which is very close to the value of $6000k_B$ obtained from atomic force micrographs. Hence the SCFT simulations can be used to extract a reliable estimate for the parameters that determine E_d from smectic elasticity theory. Our estimate is different from the number calculated by Hammond *et al.*, which may be because of differences in our use of a constrained, rather than unconstrained, simulation volume. Furthermore, they approximated $\lambda \approx 0.25R_g$ as $0.1a$, while our simulations show that a more accurate estimate is $\lambda \approx 0.06a$. The experimental results for PS-PVP$_{0.22}$ and PS-PVP$_{0.23}$ show that block copolymers with nearly equal molecular weight but different compositions can show significant differences in defect densities. To confirm if such a dependence is expected theoretically, we calculated the effect of varying the polymer composition on E_d. Figure 11 shows the variation in normalized values of Ba^3 with composition ϕ at a fixed $\chi N = 30$, as calculated using SCFT. We see that decreasing ϕ lowers Ba^3, and the decrease is sharper at lower values of ϕ, which is consistent with our experimental observations. We also studied the effect of varying χN on a block copolymer keeping the composition fixed and found that E_d can be manipulated by changing χN—an increase in χN increases the monolayer compression modulus and layer spacing, as shown in Figure 12. A power law fit for B *versus* χN results in the following form

$$\frac{B\bar{V}}{2RT} = 3.26 - 352(\chi N)^{-1.6} \quad (8)$$

This shows that, at $\chi N \sim 18$, the compression modulus for a monolayer of any block copolymer with a minority block volume fraction of 0.22 will be nearly zero. An exponential fit for $(0.05Ba^3\bar{V})/(R_gRT)$ *versus* χN from Figure 12 gives the following general form of the dependence of defect densities on χ and N for a fixed minority fraction.

$$n_d = \frac{1}{a_c^2}\exp\left[-\frac{(14 - 28\exp^{-0.04\chi N})R_g^3 N_A}{\bar{V}}\right] \quad (9)$$

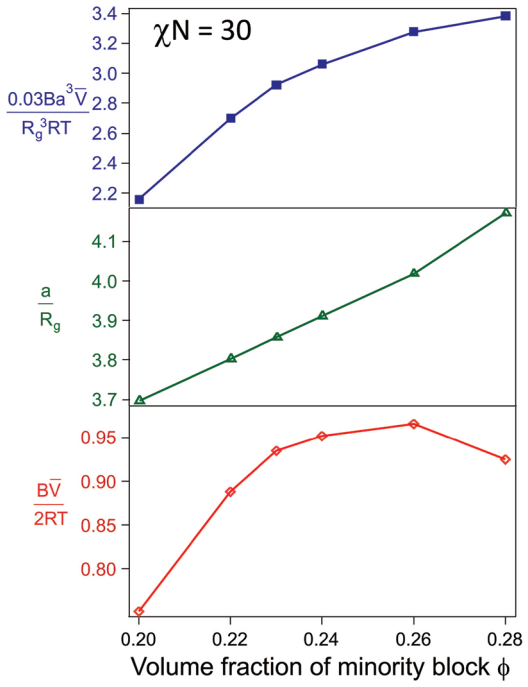

Figure 11. Change in Ba^3 (normalized) with varying composition ϕ at a fixed $\chi N = 30$. A smaller fraction of minority block ϕ leads to a decrease in the microdomain spacing and layer compression modulus, which reduces the energetic cost $\sim Ba^3$ of producing the dislocation.

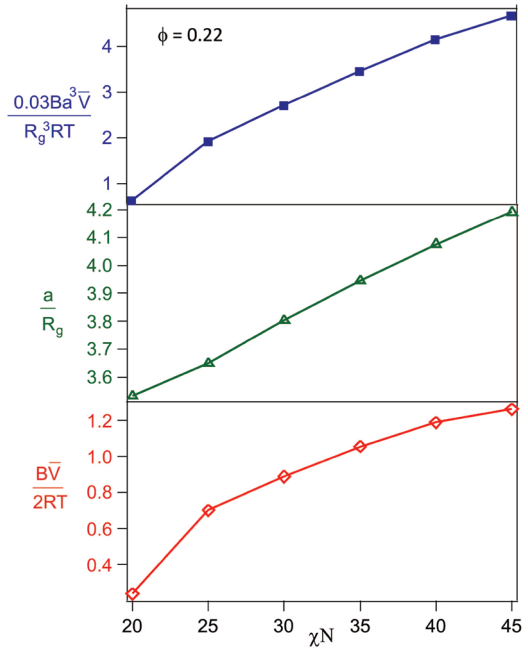

Figure 12. Effect of χN on the normalized dislocation energy for a block copolymer with a fixed composition of ϕ_{PVP} = 0.22. An increase in χN increases both a and the compression modulus B.

This shows that n_d can be manipulated by an appropriate choice of χ. For a fixed molecular weight, apart from lowering the temperature, χ can be increased by choice of suitable block copolymer components. For the PS-PVP

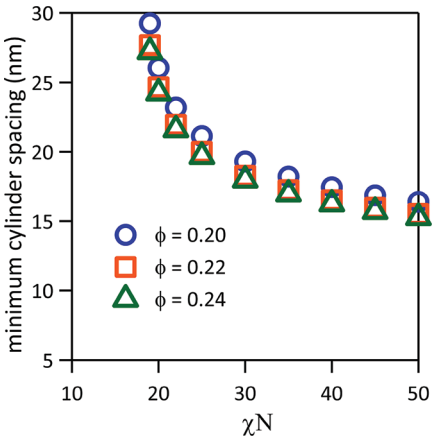

Figure 13. Estimated minimum cylinder spacing that can be obtained for a given block copolymer characterized by degree of segregation χN and volume fraction of minority block ϕ.

system used here, $\chi \sim 0.1$, which limits the minimum pitch of the patterns obtained to about 20 nm, but a poly(styrene-*b*-dimethylsiloxane) block copolymer, whose Flory–Huggins interaction parameter between the segments is about 1.5 times higher,[47] can be used to produce features smaller than that limit.

We now attempt to define a minimum cylinder spacing a_0 that can be obtained for a block copolymer characterized by degree of segregation χN and volume fraction of minority block ϕ. Since the number density of defects scales as $\exp[-E_d/k_BT]$, E_d/T should be larger than a limit to achieve a well-ordered structure at that temperature. Since E_d scales as $0.03Ba^3$, this poses a limit on the smallest a_0 that can be obtained. We assume that B can be approximated by the product of power law fits for its dependence on ϕ and χN shown in Figure 11 and Figure 12. The details of the derivation are given in the Supporting Information. Using our experimental result for a_0 = 20 nm for PS-PVP block copolymers to evaluate the proportionality constant, we obtain an approximate relation for the minimum pitch that can be obtained using cylindrical morphology block copolymer monolayers, given by eq 10. The form of the dependence on χN and ϕ is illustrated in Figure 13.

$$a_0\ (\text{nm}) = \left(\frac{25}{(\chi N - 18)^{0.167}(\phi - 0.197)^{0.027}}\right) \quad (10)$$

CONCLUSION

We have found that there is a lower limit to the microdomain spacing that can be achieved in a monolayer of any block copolymer. These results have striking implications for directed assembly block copolymer lithography. One of the advantages of block copolymer lithography is that features much smaller than the physical limit of optical lithography can be easily accessed by choosing an appropriate molecular weight. This work reveals that there is a significant downside to this strategy—when a decreases, E_d decreases significantly, which will result in a higher density of defects even well below the bulk ODT. Hence the allowable window of processing temperatures and polymer choices is shrunk drastically. We find that a possible technique to overcome this drawback is to employ block copolymers with larger values of Flory–Huggins interaction parameters. At smaller molecular weights, the sensitivity of defect densities to the film thickness and volume fractions increases substantially, which implies that a bilayer and monolayer film can have drastically different defect densities at the same temperature and slight variations in polymer compositions could lead to complete loss of order in the self-assembled patterns.

METHODOLOGY

The block copolymer employed in this study is poly(styrene-*b*-2-vinyl pyridine) (PS-P2VP) with poly(2-vinyl pyridine) as the minority block. The strong dependence of the Flory–Huggins interaction parameter between styrene and vinyl pyridine on temperature[48] (χ = 63/*T*(K) − 0.033) makes it amenable to studies of the temperature dependence of order and defects. Three block copolymers which differed in either their molecular weights or their composition were prepared by anionic polymerization, resulting in polydispersity of less than 1.1. The cylinder spacing and order–disorder transition temperature in the bulk for these block copolymers were determined by temperature-dependent small-angle X-ray scattering. Bulk samples were prepared by packing the block copolymer in a copper washer sealed using PMDA-ODA polyimide (Kapton) and a vacuum-compatible epoxy adhesive. The bulk samples were preordered in a vacuum of 10^{-6} bar by heating up to 270 °C, slowly cooled to 160 °C, and held for 1.5 days. These preannealed samples were heated to progressively higher temperatures and allowed to anneal at each temperature under continuous nitrogen overflow for 3 h before the SAXS data were collected. Bulk small-angle X-ray scattering measurements were performed at the in-house setup at the Materials Research Laboratory at UCSB. The setup is powered by a XENOCS Genix 50W X-ray microsource producing a beam size of about 0.8 by 0.8 mm and X-rays of wavelength 1.54 Å. The scattered X-ray intensity is recorded by a Bruker HI-STAR multiwire area detector and saved as a 1024 × 1024 16 bit image.

Substrate Fabrication. For thin film studies, patterned substrates for graphoepitaxy were prepared in the UCSB nanofabrication facility. Silicon oxide of desired thickness was deposited on cleaned silicon wafers using plasma-enhanced chemical vapor deposition. The deposited oxide thickness was varied to match the thickness of the monolayer or bilayer film for the different block copolymers employed in this study. The wafers were cleaned by sonicating in acetone, isopropyl alcohol, and DI water for 3 min each and baked in a convection oven at 120 °C for 1 h to remove all adsorbed water. The substrate was primed with hexamethyldisilazane (HMDS) to promote photoresist attachment and coated with AZ4110 photoresist. The wafer was then subjected to a 1 min pre-exposure bake on a hot plate at 95 °C to remove all volatile components of the photoresist, followed by exposure using a Karl Suss MJB3 contact aligner and developed in a 1:4 AZ400K/DI water solution. A 2 cm × 2 cm

array of 2 μm wide channels separated by 2 μm wide mesas was etched into the silicon oxide layer with CHF_3 gas using a Panasonic inductively coupled plasma etcher. The photoresist was removed by soaking overnight in a stripper solution held at 80 °C, followed by a 1 min oxygen plasma etch. After etching, the wafers were exposed to air, thus allowing a thin ~1.5 nm thick layer of native oxide to regrow on the silicon bottoms of the channels.

Thin Film Preparation. Polymer films with thicknesses designed to produce either a monolayer or a bilayer of cylinders were deposited on these photolithographically patterned substrates by spin coating from a well-mixed solution of the polymer in toluene. These films were then subjected to thermal annealing under high vacuum conditions by heating above the bulk ODT to erase all processing history, then slowly cooled to the annealing temperature at a rate less than 0.05 °C/min and held for more than 1.5 days. The films were then cooled at a rate faster than 0.5 °C/min to room temperature before removing from vacuum. Quenching of the samples was not performed because of the tendency of the films to dewet from the substrate because of PVP degradation when exposed to air even for a few seconds at temperatures close to 200 °C. Because of the different surface energies of the two blocks, the PVP blocks formed a brush layer next to the silicon substrate, while the PS formed the polymer−air wetting layer. The spin coating parameters were controlled such that only a brush layer was formed on the mesas after annealing, and the microdomains were located only within the channels.[49] The heights of the oxide mesas were also designed to obtain a flat polymer film after annealing. A Physical Electronics 6650 dynamic secondary ion mass spectrometry (SIMS) setup was used to etch through the film with a focused 2 keV, 40 nA O_2^+ oxygen beam that was rastered over a 300 μm by 300 μm area with simultaneous charge compensation using a 0.6 KeV electron beam. Secondary ion mass spectrometry enabled us to identify the number of cylinder layers in each film by tracking the CN^- signal, which is unique to P2VP, and to etch through the PS brush to expose the buried P2VP cylinders for imaging using atomic force microscopy (AFM).

GISAXS for Thin Films. In addition to atomic force microscopy, grazing incidence small-angle X-ray scattering (GISAXS) was used to obtain statistically representative structural data averaged over large areas.[28,30−32] In the GISAXS geometry, a well-collimated X-ray beam impinges upon the sample at a very small angle, giving rise to an elongated footprint (~1.5 cm) that results in intense scattering even from very thin films when a high-intensity synchrotron X-ray source is used. GISAXS has been shown to be a very sensitive high-resolution means to probe the fine structural details that may remain undetected using microscopy. GISAXS measurements were performed at Sector 8-IDE at the Advanced Photon Source at Argonne National Laboratory. A transmission diamond monochromator provided intense radiation of wavelength of 0.1686 nm that was focused to a beam spot size of 100 μm by 50 μm. The beam impinged upon the sample at a controlled angle of incidence, and the scattered intensity was recorded by a MAR-2 CCD area detector and stored as a 2048 × 2048 16-bit tiff image. A lead beamstop was used to block the specular beam. Each sample was first aligned with the channel walls parallel to the direction of the incident X-ray beam by rotating the sample in the azimuthal direction Φ about the sample normal. The lateral periodic structure of the gratings patterned on the substrate leads to several orders of diffraction. Intersection of the grating truncation rods with the Ewald sphere leads to a series of diffraction spots located on a semicircle when the gratings were parallel to the incoming beam.[50] A slight misalignment of the channel walls with the beam direction showed up clearly as asymmetry in this semicircle on either side of the primary beamstop. This allowed us to determine the aligned position $\Phi = 0°$ with an accuracy of 0.05°. A secondary beamstop was used to block the strong, very low angle reflections arising from the periodic pattern on the substrate. Data were collected in this nominal $\Phi = 0°$ position with two exposures per sample position, and the exposure time was varied to maximize scattering intensity without saturating the detector counts. The data

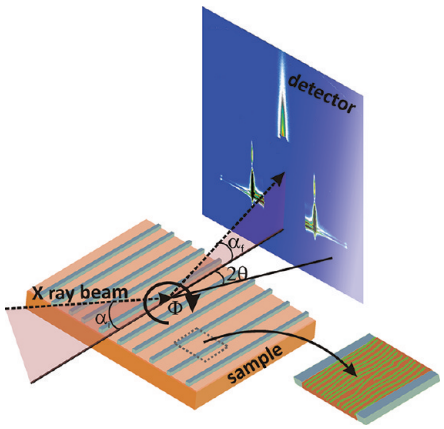

Figure 14. Schematic of the experimental setup for grazing incidence X-ray scattering.

reported in this paper were collected at an incident angle α_i of 0.18°, which is above the critical angle of the polymer but below the critical angle of the substrate, thus allowing the entire film depth to be probed. The resulting data set was converted to a map of intensity $I(2\theta,\alpha_f)$, where 2θ is the in-plane diffraction angle and α_f is the out-of-plane diffraction angle (shown in Figure 14). Data from both sides of the beamstop were collected and were corrected for possible thermal drift of the beam center to ensure symmetry on either side of the beamstop. To extract the in-plane structural data from the 2D scattering images, line integrations of intensity at low values of α_f were obtained and plotted against the in-plane wave vector $q_{||}$. The peak positions were fit to extract the in-plane microdomain spacing in the block copolymer films.

Conflict of Interest: The authors declare no competing financial interest.

Acknowledgment. We gratefully acknowledge funding from the NSF DMR Contracts DMR-07-04539 and DMR-09-04499 as well as the CSP Technologies Fellowship for partial support of V.M. Use of the MRL Facilities was supported by the MRSEC Program of the National Science Foundation under Contract No. DMR-11-21053. V.M. would like to thank Dr. Matt Hammond for helpful discussions and synthesis of two polymers used in this work, Dr. Eric Cochran and Su-mi Hur for assistance with the simulations, Prof. Axel Müller and Dr. Felix Schacher for synthesis of the third polymer used in this thesis, and the beamline scientists at Argonne National Laboratory Dr. Joseph Strzalka and Dr. Zhang Jiang for assistance during the GISAXS experiments.

Supporting Information Available: Additional material relating to fluctuations in smectics, size characterization data for the block copolymers used in this study, temperature-varying SAXS data for ODT estimation as well as AFM micrographs showing the order in bilayers of $PS\text{-}PVP_{0.22}$ as a function of temperature is available in the Supporting Information. We have also included a detailed derivation for the general form for a_0. This material is available free of charge *via* the Internet at http://pubs.acs.org.

REFERENCES AND NOTES

1. Ito, T.; Okazaki, S. Pushing the Limits of Lithography. *Nature* **2000**, *406*, 1027–1031.
2. www.itrs.net.
3. Park, M.; Harrison, C.; Chaikin, P. M.; Register, R. A.; Adamson, D. H. Block Copolymer Lithography: Periodic Arrays of $\sim 10^{11}$ Holes in 1 Square Centimeter. *Science* **1997**, *276*, 1401–1404.
4. Cheng, J. Y.; Ross, C. A.; Chan, V. Z.-H.; Thomas, E. L.; Lammertink, R. G. H.; Vancso, G. J. Formation of a Cobalt Magnetic Dot Array *via* Block Copolymer Lithography. *Adv. Mater.* **2001**, *13*, 1174–1178.

5. Black, C. T.; Guarini, K. W.; Milkove, K. R.; Baker, S. M.; Russell, T. P.; Tuominen, M. T. Integration of Self-Assembled Diblock Copolymers for Semiconductor Capacitor Fabrication. *Appl. Phys. Lett.* **2001**, *79*, 409–411.
6. Chai, J.; Wang, D.; Fan, X.; Buriak, J. M. Assembly of Aligned Linear Metallic Patterns on Silicon. *Nat. Nanotechnol.* **2007**, *2*, 500–506.
7. Zhang, X.; Murphy, J. N.; Wu, N. L. Y.; Harris, K. D.; Buriak, J. M. Rapid Assembly of Nanolines with Precisely Controlled Spacing from Binary Blends of Block Copolymers. *Macromolecules* **2011**, *44*, 9752–9757.
8. Hong, Y.-R.; Asakawa, K.; Adamson, D. H.; Chaikin, P. M.; Register, R. A. Silicon Nanowire Grid Polarizer for Very Deep Ultraviolet Fabricated from a Shear-Aligned Diblock Copolymer Template. *Opt. Lett.* **2007**, *32*, 3125–3127.
9. Caille, A. X-ray Scattering by Smectic-A Crystals. *C.R. Hebd. Seances Acad. Sci.* **1972**, *274*, 891–893.
10. Mermin, D. N. Crystalline Order in 2 Dimensions. *Phys. Rev.* **1968**, *176*, 250–254.
11. Peierls, R. E. Remarks on Transition Temperatures. *Helv. Phys. Acta* **1934**, *7*, 81–83.
12. Kim, S. O.; Solak, H. H.; Stoykovich, M. P.; Ferrier, N. J.; de Pablo, J. J.; Nealey, P. F. Epitaxial Self-Assembly of Block Copolymers on Lithographically Defined Nanopatterned Substrates. *Nature* **2003**, *424*, 411–414.
13. Segalman, R. A.; Yokoyama, H.; Kramer, E. J. Graphoepitaxy of Spherical Domain Block Copolymer Films. *Adv. Mater.* **2001**, *13*, 1152–1155.
14. Morkved, T. L.; Lu, M.; Urbas, A. M.; Ehrichs, E. E.; Jaeger, H. M.; Mansky, P.; Russell, T. P. Local Control of Microdomain Orientation in Diblock Copolymer Thin Films with Electric Fields. *Science* **1996**, *273*, 931–933.
15. Pelletier, V.; Adamson, D. H.; Register, R. A.; Chaikin, P. M. Writing Mesoscale Patterns in Block Copolymer Thin Films through Channel Flow of a Nonsolvent Fluid. *Appl. Phys. Lett.* **2007**, *90*, 163105.
16. Angelescu, D. E.; Waller, J. H.; Adamson, D. H.; Deshpande, P.; Chou, S. Y.; Register, R. A.; Chaikin, P. M. Macroscopic Orientation of Block Copolymer Cylinders in Single-Layer Films by Shearing. *Adv. Mater.* **2004**, *16*, 1736–1740.
17. Sundrani, D.; Sibener, S. J. Spontaneous Spatial Alignment of Polymer Cylindrical Nanodomains on Silicon Nitride Gratings. *Macromolecules* **2002**, *35*, 8531–8539.
18. Ruiz, R.; Sandstrom, R. L.; Black, C. T. Induced Orientational Order in Symmetric Diblock Copolymer Thin Films. *Adv. Mater.* **2007**, *19*, 587–591.
19. Harrison, C.; Cheng, Z. D.; Sethuraman, S.; Huse, D. A.; Chaikin, P. M.; Vega, D. A.; Sebastian, J. M.; Register, R. A.; Adamson, D. H. Dynamics of Pattern Coarsening in a Two-Dimensional Smectic System. *Phys. Rev. R* **2002**, *66*, 011706.
20. Hammond, M. R.; Cochran, E.; Fredrickson, G. H.; Kramer, E. J. Temperature Dependence of Order, Disorder, and Defects in Laterally Confined Diblock Copolymer Cylinder Monolayers. *Macromolecules* **2005**, *38*, 6575–6585.
21. Segalman, R. A.; Hexemer, A.; Hayward, R. C.; Kramer, E. J. Ordering and Melting of Block Copolymer Spherical Domains in 2 and 3 Dimensions. *Macromolecules* **2003**, *36*, 3272–3288.
22. Harrison, C.; Adamson, D. H.; Cheng, Z.; Sebastian, J. M.; Sethuraman, S.; Huse, D. A.; Register, R. A.; Chaikin, P. M. Mechanisms of Ordering in Striped Patterns. *Science* **2000**, *290*, 1558–1560.
23. Cheng, J.; Mayes, A. M.; Ross, C. A. Nanostructure Engineering by Templated Self-Assembly of Block Copolymers. *Nat. Mater.* **2004**, *3*, 823–828.
24. Kim, S. O.; Kim, B. H.; Kim, K.; Koo, C. M.; Stoykovich, M. P.; Nealey, P. F.; Solak, H. H. Defect Structure in Thin Films of a Lamellar Block Copolymer Self-Assembled on Neutral Homogeneous and Chemically Nanopatterned Surfaces. *Macromolecules* **2006**, *39*, 5466–5470.
25. Bita, I.; Yang, J. K. W.; Jung, Y. S.; Ross, C. A.; Thomas, E. L.; Berggren, K. K. Graphoepitaxy of Self-Assembled Block Copolymers on Two-Dimensional Periodic Patterned Templates. *Science* **2008**, *321*, 939–943.
26. Park, S.; Lee, D. H.; Xu, J.; Kim, B.; Hong, S. W.; Jeong, U.; Xu, T.; Russell, T. P. Macroscopic 10-Terabit-per-Square-Inch Arrays from Block Copolymers with Lateral Order. *Science* **2009**, *323*, 1030–1033.
27. Angelescu, D. E.; Waller, J. H.; Adamson, D. H.; Register, R. A.; Chaikin, P. M. Enhanced Order of Block Copolymer Cylinders in Single-Layer Films Using a Sweeping Solidification Front. *Adv. Mater.* **2007**, *19*, 2687–2690.
28. Stein, G. E.; Kramer, E. J.; Li, X. F.; Wang, J. Layering Transitions in Thin Films of Spherical-Domain Block Copolymers. *Macromolecules* **2007**, *40*, 2453–2460.
29. Mishra, V.; Hur, S. M.; Cochran, E. W.; Stein, G. E.; Fredrickson, G. H.; Kramer, E. J. Symmetry Transition in Thin Films of Diblock Copolymer/Homopolymer Blends. *Macromolecules* **2010**, *43*, 1942–1949.
30. Rauscher, M.; Salditt, T.; Spohn, H. Small-Angle X-ray Scattering under Grazing Incidence: The Cross Section in the Distorted-Wave Born Approximation. *Phys. Rev. B* **1995**, *52*, 16855–16863.
31. Holy, V.; Pietsch, U.; Baumbach, T. *High Resolution X-ray Scattering from Thin Films and Multilayers*, Springer Tracts in Modern Physics; Springer: Berlin, 1999.
32. Lee, B.; Park, I.; Yoon, J.; Park, S.; Kim, J.; Kim, K. W.; Chang, T.; Ree, M. Structural Analysis of Block Copolymer Thin Films with Grazing Incidence Small-Angle X-ray scattering. *Macromolecules* **2005**, *38*, 4311–4323.
33. Hammond, M. R.; Kramer, E. J. Edge Effects on Thermal Disorder in Laterally Confined Diblock Copolymer Cylinder Monolayers. *Macromolecules* **2006**, *39*, 1538–1544.
34. Mishra, V. Ph.D. Thesis, University of California Santa Barbara, 2011.
35. Knoll, A.; Tsarkova, L.; Krausch, G. Nanoscaling of Microdomain Spacings in Thin Films of Cylinder-Forming Block Copolymers. *Nano Lett.* **2007**, *7*, 843–846.
36. Mishra, V.; Fredrickson, G. H.; Kramer, E. J. SCFT Simulations of an Order−Order Transition in Thin Films of Diblock and Triblock Copolymers. *Macromolecules* **2011**, *44*, 5473–5480.
37. Khanna, V.; Cochran, E. W.; Hexemer, A.; Stein, G. E.; Fredrickson, G. H.; Kramer, E. J.; Li, X.; Wang, J.; Hahn, S. F. Effect of Chain Architecture and Surface Energies on the Ordering Behavior of Lamellar and Cylinder Forming Block Copolymers. *Macromolecules* **2006**, *39*, 9346–9356.
38. Dormidontova, E. E.; Lodge, T. P. The Order−Disorder Transition and the Disordered Micelle Regime in Sphere-Forming Block Copolymer Melts. *Macromolecules* **2001**, *34*, 9143–9155.
39. Chandrasekhar, S.; Ranganath, G. The Structure and Energetics of Defects in Liquid Crystals. *Adv. Phys.* **1986**, *35*, 507.
40. Amundson, K.; Helfand, E. Quasi-static Mechanical Propoerties of Lamellar Block Copolymer Microstructure. *Macromolecules* **1993**, *26*, 1324–1332.
41. Pershan, P. S. Dislocation Effects in Smectic-Liquid-Crystals. *Jpn. J. Appl. Phys.* **1974**, *45*, 1590–1604.
42. de Gennes, P. G. *The Physics of Liquid Crystals*; Clarendon Press: Oxford U.K., 1974.
43. de Gennes, P. G. An Analogy between Superconductors and Smectics-A. *Solid State Commun.* **1972**, *10*, 753–756.
44. Kosterlitz, J. M.; Thouless, D. J. Ordering, Metastability and Phase Transitions in 2 Dimensional Systems. *J. Phys. C* **1973**, *6*, 1181–1203.
45. Chandrasekhar, S.; Sadashiva, B. K.; Suresh, K. A. Liquid-Crystals of Disc-like Molecules. *Pramana* **1977**, *9*, 471–480.
46. Toner, J.; Nelson, D. Smectic, Cholesteric, and Rayleigh-Benard Order in Two Dimensions. *Phys. Rev. B* **1981**, *23*, 316–334.
47. Balsara, N. P. *Thermodynamics of Polymer Blends: Physical Properties of Polymers Handbook*; AIP Press: New York, 1996.
48. Dai, K. H.; Kramer, E. J. Determining the Temperature-Dependent Flow Interaction Parameter for Strongly Immiscible Polymers from Block Copolymer Segregation Measurements. *Polymer* **1994**, *35*, 157–162.

49. Segalman, R. A.; Schaefer, K. E.; Fredrickson, G. H.; Kramer, E. J.; Magonov, S. Topographic Templating of Islands and Holes in Highly Asymmetric Block Copolymer Films. *Macromolecules* **2003**, *36*, 4498–4506.
50. Yan, M.; Gibaud, A. On the Intersection of Grating Truncation Rods with the Ewald Sphere Studied by Grazing-Incidence Small-Angle X-ray Scattering. *J. Appl. Crystallogr.* **2007**, *40*, 1050–1055.